Observation of multiple steady states with engineered dissipation

npj | quantum information

Article

Published in partnership with The University of New South Wales

https://doi.org/10.1038/s41534-025-00958-6

Observation of multiple steady states with engineered dissipation

Li Li[1,2,8], Tong Liu[1,3,8] ✉, Xue-Yi Guo[1], He Zhang[1,2], Silu Zhao[1,2], Zheng-An Wang[4], Zhongcheng Xiang[1,2,4,5,6,7], Xiaohui Song[1,4,5], Yu-Xiang Zhang[1,2,5], Kai Xu[1,2,4,5,6,7], Heng Fan[1,2,4,5,6,7] & Dongning Zheng[1,2,5,6,7]

Simulating the dynamics of open quantum systems is essential in achieving practical quantum computation and understanding novel nonequilibrium behaviors. However, quantum simulation of a many-body system coupled to an engineered reservoir has yet to be fully explored in present-day experiment platforms. In this work, we introduce engineered noise into a one-dimensional ten-qubit superconducting quantum processor to emulate a generic many-body open quantum system. Our approach originates from the stochastic unravellings of the master equation. By measuring the end-to-end correlation, we identify multiple steady states stemmed from a strong symmetry, which is established on the modified Hamiltonian via Floquet engineering. Furthermore, we investigate the structure of the steady-state manifold by preparing initial states as a superposition of states within different sectors on a five-qubit chain. Our work provides a manageable and hardware-efficient strategy for the open-system quantum simulation.

The interplay between coherent and dissipative dynamics within a physical system leads to the emergence of exotic nonequilibrium phenomena, such as dissipation phase transition[1–5] and dissipative time crystals[6–9]. While an open system typically exhibits a single steady state, prior studies have demonstrated that multiple steady states are possible if there are symmetries preserved by the dissipation[10–14]. Such remained symmetries also enable control over nonequilirbrium quantum transport[15–17]. Furthermore, the multiple steady states can span a stabilized manifold, which has significant applications in passive quantum error correction, crucial for quantum information processing[18–23]. However, attaining multiple steady states generally requires sophisticated dissipative channels in most existing models, necessitating special experimental configurations. Recently, theoretical investigations have unveiled that systems with only one-photon pump and loss can also manifest multiple steady states[24,25]. This finding motivates us to experimentally observe this phenomenon using near-term quantum simulation platforms.

Superconducting circuits, owing to their high flexibility and scalability, have achieved notable success in the simulation of quantum many-body systems, including many-body localization[26], quantum many-body scar states[27], discrete-time crystals[28], information scrambling[29], and entanglement phase transition[30]. Most of the existing works are restricted to closed systems. To simulate an open system, previous research has employed two distinct approaches. The first method embeds the system into a larger closed system where the complement acts as the environment, resulting in a substantial increase in the overhead of qubits and gates[31–33]. The second approach integrates lossy components into customized circuits to introduce dissipation intentionally[34–39]. However, the dissipation strength and position of the lossy components often lack tunability, and this approach deviates from the long-term goal of developing highly coherent devices capable of universal quantum computation. Therefore, an efficient method to simulate dissipative dynamics using a universal quantum processor is highly desirable.

Here, we report our experiment in probing multiple steady states induced by a strong symmetry on a one-dimensional superconducting quantum processor with nine qubits, as shown in Fig. 1. Each qubit used in the experiment is labeled by Q_i with $i \in \{1, 2, \ldots, 9\}$, and can be addressed by individual control lines. Based on the interpretation of open quantum dynamics in terms of stochastic wave functions, we engineer a stochastic Hamiltonian to mimic the evolution featuring controllable dissipation by averaging over a set of unitary evolutions. The dissipation is applied to the central qubit to generate multiple steady states[24,25]. Our protocol can be efficiently extended to multiple dissipations on the current noisy

[1]Institute of Physics, Chinese Academy of Sciences, Beijing, 100190, China. [2]School of Physical Sciences, University of Chinese Academy of Sciences, Beijing, 100190, China. [3]Department of Microtechnology and Nanoscience, Chalmers University of Technology, Gothenburg, 41296, Sweden. [4]Beijing Academy of Quantum Information Sciences, Beijing, 100193, China. [5]Hefei National Laboratory, Hefei, 230088, China. [6]CAS Center of Excellence for Topological Quantum Computation, University of Chinese Academy of Sciences, Beijing, 100190, China. [7]Songshan Lake Materials Laboratory, Dongguan, 523808 Guangdong, China. [8]These authors contributed equally: Li Li, Tong Liu. ✉e-mail: liutong181@mails.ucas.ac.cn

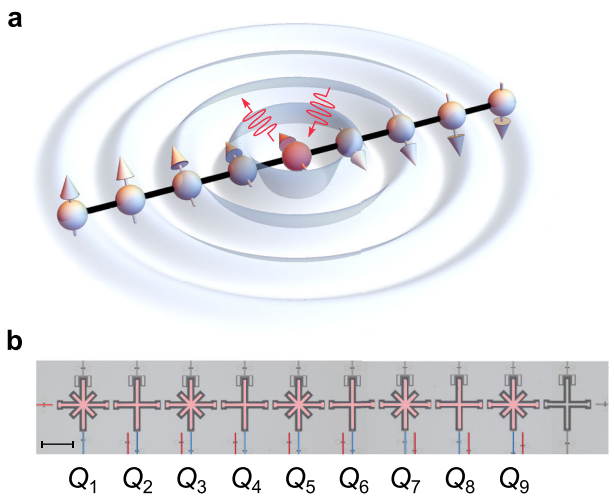

Fig. 1 | Spin chain with a local dissipation and device. a An array of nine qubits with nearest-neighbor couplings. The dissipation on the center qubit impels the system to steady states with long-range coherence. **b** Optical picture of the ten-qubit superconducting quantum processor with highlighting circuit elements. Qubits (pink) are labeled from Q_1 to Q_9 and can be controlled by individual microwave signals through the red and blue lines. Scale bar in the lower left corner, 0.2 mm.

intermediate-scale quantum devices without the need for ancillary qubits or lossy elements. We also incorporate the Floquet engineering to mitigate the undesired next-nearest-neighbor (NNN) couplings and modify nearest-neighbor (NN) coupling strengths to preserve the symmetry[40–42]. By initializing the system in distinct symmetry sectors with high-fidelity gates, we show that the system evolves to different steady states specified by the end-to-end correlation. Our results demonstrate that superconducting circuits are a promising platform to explore exotic properties of open many-body systems benefiting from their high flexibility and manipulability.

Results

Engineered dissipation

We start with the simulation of the following Lindblad master equation (LME) of a single qubit[10,11],

$$\dot{\rho} = \sum_{j=1,2} L_j \rho L_j^\dagger - \frac{1}{2}\{L_j^\dagger L_j, \rho\}, \tag{1}$$

where ρ is the density matrix of the qubit, $L_1 = \sqrt{\gamma_+}\sigma^+ = \sqrt{\gamma_+}|e\rangle\langle g|$ and $L_2 = \sqrt{\gamma_-}\sigma^- = \sqrt{\gamma_-}|g\rangle\langle e|$ are pump and loss operators, respectively, with γ_+ (γ_-) being the pump (loss) rate, and $|g\rangle$ ($|e\rangle$) is the ground (excited) state of qubit. Here, we set $\gamma_+ = \gamma_- = \gamma$. A more general case ($\gamma_- > \gamma_+$) is discussed in Supplementary Note 4. Now Eq. (1) can be rewritten as $\dot{\rho} = \frac{\gamma}{2}\left(\sigma^x\rho\sigma^x + \sigma^y\rho\sigma^y - 2\rho\right)$, which reminds us of that ρ is the ensemble average of stochastic wave function $|\psi\rangle$, i.e., $\rho = \overline{|\psi\rangle\langle\psi|}$, with the overline denoting the average over stochastic realizations[43–45]. The stochastic wave function $|\psi\rangle$ is governed by the following stochastic Schrödinger equation (SSE) with $\hbar = 1$

$$i\frac{d}{dt}|\psi\rangle = H_S(t)|\psi\rangle = \sqrt{\frac{\gamma}{2}}\left[\xi_1(t)\sigma^x + \xi_2(t)\sigma^y\right]|\psi\rangle, \tag{2}$$

where $\xi_1(t)$ and $\xi_2(t)$ are two independent real Gaussian processes satisfying $\overline{\xi_\alpha(t)\xi_\beta(t')} = \delta_{\alpha\beta}\delta(t-t')$ and $\overline{\xi_\alpha} = 0$ for $\alpha, \beta = 1, 2$.

Although $H_S(t)$ is a Hermitian Hamiltonian, the faithful generation of ideal Gaussian processes in Eq. (2) is infeasible in experiments due to the finite bandwidth of arbitrary wave generators. Inspired by the numerical techniques of differential equations, we adopt Euler's method to simulate Eq. (2) by slicing each trajectory into N sections divided by time intervals of a small duration Δt. The evolution of the wave function in the ith section $|\psi_i(t)\rangle$ is given by

$$i\frac{d}{dt}|\psi_i(t)\rangle = \sqrt{\frac{\gamma}{2\Delta t}}\left[\eta_1^i\sigma^x + \eta_2^i\sigma^y\right]|\psi_i(t)\rangle, \tag{3}$$

with the initial condition $|\psi_i(0)\rangle = |\psi_{i-1}(\Delta t)\rangle$, where η_1^i and η_2^i are two random variables following a discrete distribution $P(\eta_{1(2)} = 1) = P(\eta_{1(2)} = -1) = 1/2$. We mention that while Eq. (3) is not strictly equivalent to Eq. (2), it can approximate Eq. (2) within each segment by neglecting high-order infinitesimal terms (see Methods). By sampling $2N$ variables $\{\eta_1^1, \ldots, \eta_1^N, \eta_2^1, \ldots, \eta_2^N\}$, we can determine a trajectory and apply corresponding driving pulses to the target qubit, as described in Eq. (3). Note that the amplitude of pulses are kept fixed while the phase in each section is uniformly chosen from $\{\pi/4, 3\pi/4, 5\pi/4, 7\pi/4\}$. The mapping between the amplitude of the driving pulse and γ can be calibrated via the Rabi oscillation, where we apply a rectangular driving pulse to the qubit initialized as $|g\rangle$, and measure the excitation probability P_e versus the driving pulse length T, as shown in Fig. 2a. After sampling M trajectories, the dynamics of an observable O can be estimated by $\sum_{j=1}^{M}\langle\psi^{(j)}|O|\psi^{(j)}\rangle/M$ where $|\psi^{(j)}\rangle$ is the jth trajectory.

We verify our scheme on qubit Q_5 by measuring the evolution of $\sigma^z \equiv |e\rangle\langle e| - |g\rangle\langle g|$ from two initial states $|g\rangle$ and $|e\rangle$ with $\Delta t = 7.5$ ns, $\gamma = 0.4$ MHz, and $M = 100$, as illustrated in Fig. 2b. The results are presented in Fig. 2c and compared with numerical results calculated by LME and SSE. We find that the experiment results are in good agreements with simulations in a duration of 2.5 μs, and converge to a steady state ρ_{ss} in which $\langle\sigma^z\rangle = 0$ irrespective of the initial states chosen.

Strong symmetry and Floquet engineering

We have demonstrated the experimental realization of dissipative dynamics with equal pump and loss rates on a single qubit, where the steady state is a thermal state $(|0\rangle\langle 0| + |1\rangle\langle 1|)/2$. However, when the same dissipation is applied to the center spin of an XX chain with reflection symmetry, the combination of the Hamiltonian and dissipation gives rise to multiple long-range steady states within the chain[24,25]. The Hamiltonian part reads

$$H = \sum_{i=1}^{L-1} J_{i,i+1}(\sigma_i^+\sigma_{i+1}^- + \sigma_i^-\sigma_{i+1}^+), \tag{4}$$

where L is the length of the chain, $\sigma_i^+(\sigma_i^-)$ is pump (loss) operator at site i, and $J_{i,i+1}$ is the nearest-neighbor (NN) interaction strength with $J_{i,i+1} = J_{L-i,L+1-i}$. Considering the dissipation at the center spin, the dynamics of the entire chain's density matrix ρ is governed by the following Lindblad master equation

$$\begin{aligned}\dot{\rho} = \mathcal{L}(\rho) = -i[H,\rho] + \gamma\big(&\sigma_m^+\rho\sigma_m^- - \tfrac{1}{2}\{\sigma_m^-\sigma_m^+,\rho\} \\ &+ \sigma_m^-\rho\sigma_m^+ - \tfrac{1}{2}\{\sigma_m^+\sigma_m^-,\rho\}\big)\end{aligned} \tag{5}$$

where $m = (L+1)/2$ is the index of the center spin and $\mathcal{L}$ is the super-operator corresponding to the dissipative process.

The emergence of multiple steady states is rooted in a hidden symmetry associated with the operator C^2, which confines the dynamics within distinct symmetry sectors. The operator $C = -1/2 + \sum_{k=1}^{L} f_k^\dagger f_{L+1-k}$ where $f_k = e^{i\pi\sum_{j<k}\sigma_j^+\sigma_j^-}\sigma_k^-$ represents the fermionic operator at site k derived via the Jordan–Wigner transformation[46]. Since $[H, C] = 0$ and $\sigma_m^{+(-)}C = C\sigma_m^{+(-)} = -C$, both the Hamiltonian and the jump operators commute with C^2, generating a strong symmetry. In closed quantum systems, symmetries decouple the dynamics into independent subspaces, and similarly, in open quantum systems, this strong symmetry ensures that the

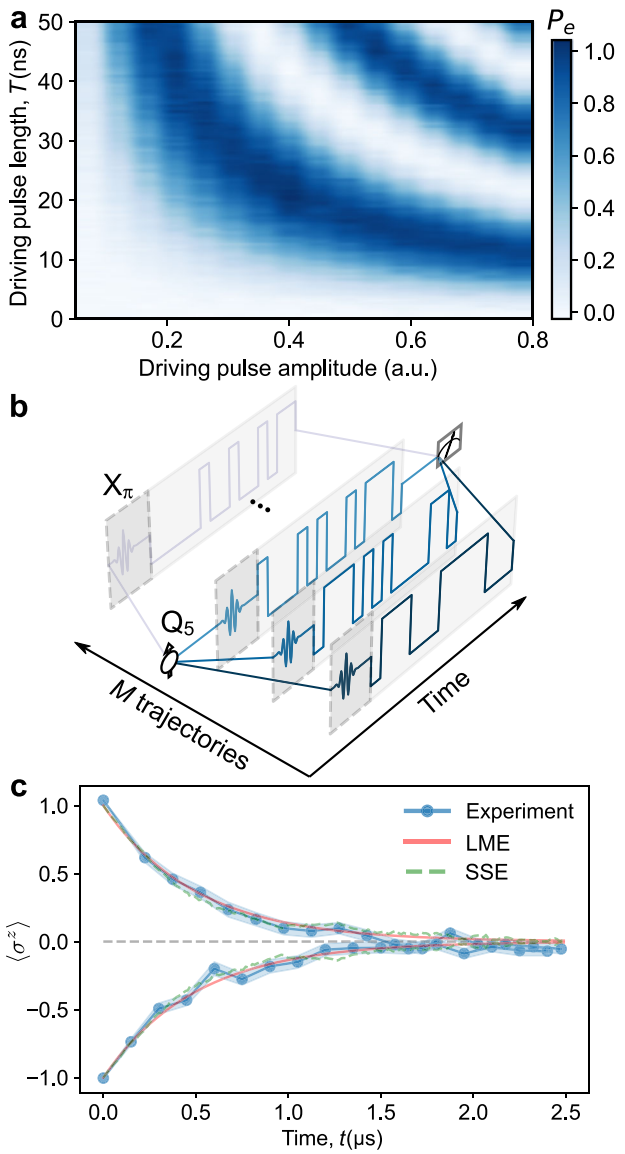

Fig. 2 | Simulation of the Lindblad master equation Eq. (1). a The Rabi oscillation for calibrating the driving pulse amplitude. The qubit is initialized in the $|g\rangle$ state, and we measure the probability of the $|e\rangle$ state oscillating over the driving time at different driving amplitudes. **b** A schematic of the driving pulse sequences for M trajectories. The driving amplitude during each Δt is randomly sampled from two discrete values for each trajectory. **c** The evolutions of $\langle\sigma^z\rangle$ in the experiment after 100 repetitions, governed by the Lindblad master equation, and simulated by the stochastic Schrödinger equation. The upper (lower) branch of evolution corresponds to the initial state $|e\rangle$ ($|g\rangle$). The shaded light blue region represents the standard error of the mean over trajectories in the experiment.

eigenspaces of C^2 evolve independently, guaranteeing at least one steady state within each sector[12].

The Hamiltonian of our one-dimensional processor shown in Fig. 1b is given by

$$H_{\rm exp} = \sum_{i=1}^{9} -\frac{\omega_i}{2}\sigma_i^z + \sum_{i=1}^{8}(J_{i,i+1}\sigma_i^+\sigma_{i+1}^- + \text{h.c.}) + \sum_{i=1}^{7}(J_{i,i+2}\sigma_i^+\sigma_{i+2}^- + \text{h.c.}), \quad (6)$$

where ω_i represents the transition frequency between the $|g\rangle$ and $|e\rangle$ states of qubit Q_i, and coupling terms describe the interactions between NN or NNN qubits. The aforementioned symmetry is broken by the inclusion of the NNN interaction term, despite the NNN interactions strength $J_{i,i+2}/2\pi \simeq 1$ MHz in our device being an order of magnitude smaller than the NN interaction strength $J_{i,i+1}/2\pi \simeq 10$ MHz. The NNN interactions can be suppressed via Floquet engineering as illustrated in Fig. 3a[40–42]. The transition frequencies of the qubits are adjustable by applying external magnetic fluxes. For the nine qubits, the transition frequencies $\omega_i/2\pi$ are set to three distinct values: 4.33, 4.54, and 4.66 GHz. This frequency alignment effectively turns off the NNN interactions (indicated by the red dashed lines in Fig. 3a) between qubit pairs Q_1-Q_3, Q_3-Q_5, Q_5-Q_7, and Q_7-Q_9 through large frequency detuning. Then we apply sinusoidal ac magnetic fluxes to modulate the frequencies of Q_2, Q_4, Q_6, and Q_8 as $\tilde{\omega}_i(t) \approx \omega_i + \varepsilon_i \sin(\nu_i t + \phi_i)$ for i = 2, 4, 6 and 8, with ε_i, ν_i, and ϕ_i being the modulation amplitude, frequency, and phase, respectively (see Supplementary Note 5). We also apply amended DC pulses to the modulated qubits to compensate the shifts of the frequency, arising from the nonlinearity of the relationship between flux and frequency. When the modulation frequency ν_i is far larger than the NN interaction strength $J_{i,i+1}$, the rapid oscillation induces a set of sidebands $\omega_i + m\nu_i$, where m is an integer. To initiate the interactions between adjacent qubits with distinct frequencies, the modulation frequencies ν_i are equal to the frequency detuning $\Delta/2\pi = |\omega_i - \omega_{i+1}|/2\pi = 210$ MHz or $|\omega_i - \omega_{i-1}|/2\pi = 330$ MHz. The modulation amplitudes ε_i are tuned to rectify the minor coupling disorder in the processor, ensuring that the NN interaction strengths remain primarily symmetric. The first sidebands of Q_2 (Q_6) and Q_4 (Q_8) coincide, but the resulting NNN interaction is weak enough to allow for the observation of different multiple steady states (see Methods and Supplementary Note 6). The remaining NNN interaction between Q_4 and Q_6 retains the symmetry as both qubits are equidistant from Q_5[24].

Preparation of initial states in different symmetry sectors

To observe the different steady states, the initial state must be prepared within the diverse eigenspaces of C^2. The eigenstate of C is expressed as $|\{\nu_{k,\pm}, n_0\}\rangle = (f_0^\dagger)^{n_0}\prod_{k=1}^{l}\prod_{s=\pm}(a_{k,s}^\dagger)^{\nu_{k,s}}|0\rangle$ with eigenvalue $\lambda = \sum_{k=1}(\nu_{k,+} - \nu_{k,-}) + n_0 - 1/2$, where $|0\rangle$ is the vacuum state, $a_{k,\pm} = (f_k \pm f_{L+1-k})/\sqrt{2}$, $l = (L-1)/2$, and $\nu_{k,\pm} \in \{0, 1\}$ for $k = 1, \ldots, l$[24]. n_0 denotes the number of excitations at the central site, taking values of either 0 or 1, and $\nu_{k,s}$ quantifies the number of Bell pairs resembling $(|01\rangle + s|10\rangle)/\sqrt{2}$ generated by $a_{k,s}^\dagger$ at sites k and $L+1-k$. Consequently, λ can adopt $2(l+1)$ distinct values $\{\pm(\eta + 1/2)\}$ with $\eta = 0, 1, \ldots, l$. C^2 shares the same eigenstates with C but possesses $(l+1)$ distinguishable eigenvalues $(\eta + 1/2)^2$. Considering the degeneracy of eigenvalues, it is available to traverse all eigenspaces of C^2 by increasing $\nu_{k,-}$ from 0 to l with $n_0 = 0$ and $\nu_{k,+} = 0$ for $k = 1, \ldots, l$. Hence, by defining Bell state creating operators between qubits Q_{l-k+1} and Q_{L-l+k}, denoted as $b_{k,\pm}^\dagger = (\sigma_{l-k+1}^+ \pm \sigma_{L-l+k}^+)/\sqrt{2}$ for $k = 1, \ldots, l$, we can generate $(l+1)$ states $\{|\phi_\eta\rangle\}$ belonging to distinct symmetry sectors

$$|\phi_0\rangle \equiv \bigotimes_{j=1}^{L}|g_j\rangle,\ |\phi_\eta\rangle \equiv \prod_{k=1}^{\eta} b_{k,(-)^k}^\dagger|\phi_0\rangle,\ \eta = 1, \ldots, l, \quad (7)$$

where $|g_j\rangle$ is the ground state of Q_j. Exploiting the circuit shown in Fig. 3b, we implement $|\phi_1\rangle$ with state fidelity more than 99.9% characterized by the quantum state tomography in our processor[47]. The $R_z(\theta)$ gate in the circuit is defined as $R_z(\theta) \equiv \exp(-i\sigma^z\theta/2)$ to tune the phase of Bell state $|\Psi(\varphi)\rangle \equiv \frac{1}{\sqrt{2}}(|e_l, g_{l+2}\rangle + e^{i\varphi}|g_l, e_{l+2}\rangle)\bigotimes_{j\neq l,l+2}^{L}|g_j\rangle$ as $\varphi = 0$ or $\varphi = \pi$, corresponding to symmetry sectors $\eta = 0$ or $\eta = 1$, respectively. We also implement $|\phi_2\rangle$ and $|\phi_3\rangle$ by repeating generating Bell states with staggered phases through the same circuit and iSWAP gates (see Supplementary Note 3).

Figure 3c shows the single excitation density distribution $\langle n_i\rangle \equiv (1 + \langle\sigma_j^z\rangle)/2$ launched from $|\phi_1\rangle$ under the periodic driving, where two excitations propagate towards two opposite directions with the same velocity due to the reflection symmetry, and swing between the boundary qubit and the center qubit Q_5. The occupation number of the center qubit is always nearly zero because of the destructive interference of two excitations,

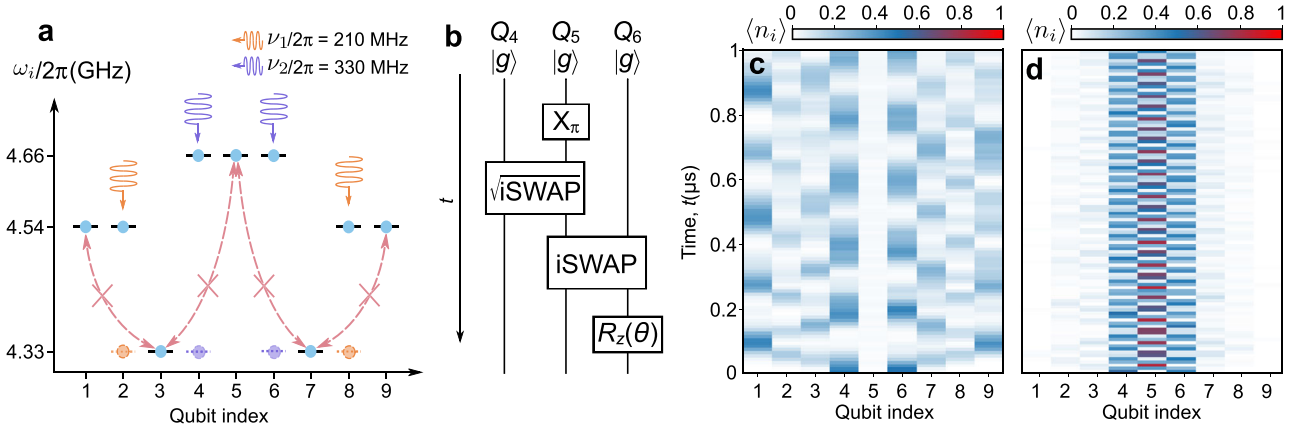

Fig. 3 | Floquet engineering and the evolution of a pair of Bell state in a 1D array with nine qubits. a Transition frequencies and flux modulations of nine qubits. Blue circles represent the transition frequencies of nine qubits, while orange or purple circles of qubits Q_2, Q_4, Q_6, and Q_8 denote the first sideband frequencies induced by the ac fluxes. The red dashed lines with crosses represent the suppressed next-nearest-neighbor interactions under this specific frequency arrangement since the frequency detuning is far larger than the interaction strength (see Methods and Supplementary Note 6). **b** The digital circuit prepares a Bell state between Q_4 and Q_6. First, an X_π gate flips Q_5 to the $|e\rangle$ state. A $\sqrt{\text{iSWAP}}$ gate then entangles Q_4 and Q_5 to create a Bell pair. The subsequent iSWAP gate transfers the Bell state from Q_5 to Q_6. Finally, an $R_z(\theta)$ gate is applied to fine-tune the phase of the Bell state. **c**, **d** The time evolution of the density distribution $\langle n_i\rangle$ with Floquet engineering. The initial state is a Bell state between Q_4 and Q_6 with Bell phase $\varphi = \pi$ or $\varphi = 0$.

which can also be understood by the fact that the state with $n_0 = 1$ belonging to the symmetry sector $\eta = 0$ is excluded from the eigenspace of symmetry sector $\eta = 1$. On the contrary, when the phase of the initial Bell state is zero, two excitations are almost confined between Q_4 and Q_6 in Fig. 3d, which arises from the non-uniform effective interaction strengths between NN qubits. This phenomenon additionally facilitates the calibration of both the Bell state phase and the modulation phase ϕ_i in the experiment (see Supplementary Note 9).

Characterization of multiple steady states

Now, we examine the dynamics of the system in the presence of dissipation where $\gamma = 3$ MHz, specifically applied to Q_5 in the following context. Following the preparation of initial states using the circuit shown in Fig. 3b, we rearrange all qubits, activate ac magnetic fluxes, and introduce engineered noises to qubit Q_5. Then, we track the evolution of the end-to-end correlation $\langle\sigma_1^z\sigma_L^z\rangle$ from three initial states by performing joint readouts of the qubits located at the ends of the nine-qubit chain, as shown in Fig. 4a, where we sample ten trajectories for each evolution. For the initial states $|\phi_0\rangle$ and $|\Psi(0)\rangle$, which hold different numbers of excitation but belong to the same sector $\eta = 0$, $\langle\sigma_1^z\sigma_L^z\rangle$ tends to the steady value $\langle\sigma_1^z\sigma_L^z\rangle_{\text{st}}^0 = 1/L$, or 1/9 for $L = 9$[24], indicated by the upper gray dashed line in the Fig. 4a. For the other initial state $|\Psi(\pi)\rangle$ in the sector $\eta = 1$, $\langle\sigma_1^z\sigma_N^z\rangle$ tends to the steady value $\langle\sigma_1^z\sigma_L^z\rangle_{\text{st}}^1 = (l-4)/Ll$, or 0 for $L = 9$[24] indicated by the lower gray dashed line. The experimental results are consistent with the numerical simulations involving the energy relaxation time T_1 = 30 μs and Ramsey dephasing time T_ϕ = 20 μs for each qubit. In Fig. 4b, we show the numerical results simulated with the Hamiltonian built from the original device parameters without Floquet engineering. All three lines rapidly converge to zero owing to the vanishing of the symmetry.

Finally, we explore the structure of degenerate steady states using 5 qubits $\{Q_3, Q_4, Q_5, Q_6, Q_7\}$ with the other qubits being far off-resonant. The steady value $\langle\sigma_1^z\sigma_L^z\rangle_{\text{st}}(\varphi)$ corresponding to the initial state $|\Psi(\varphi)\rangle$ on a five-qubit chain is expected as $\cos\varphi/5$, derived from the combination of $\langle\sigma_1^z\sigma_L^z\rangle_{\text{st}}^0$ and $\langle\sigma_1^z\sigma_L^z\rangle_{\text{st}}^1$ (see Supplementary Note 11). The experimental results are shown in Fig. 5a where we increase the initial phase φ from 0 to π in increments $\pi/8$ by the $R_z(\theta)$ gate. The evolution from the state $|\Psi(\varphi)\rangle$ tends to a steady value between two extreme steady values $\langle\sigma_1^z\sigma_L^z\rangle_{\text{st}}^0$ and $\langle\sigma_1^z\sigma_L^z\rangle_{\text{st}}^1$. In Fig. 5b, we collect the values of $\langle\sigma_1^z\sigma_L^z\rangle$ evaluated at t_e = 1.4, 1.7, and 2 μs for different initial phases. The data collected at t_e = 1.7 μs is closest to the ideal result. Due to the accumulated decoherence errors, the end-to-end correlations at t_e = 2 μs are smaller than those at t_e = 1.7 μs, but the feature of the cosine function remains. These observations demonstrate that the phase information stored in the initial state can be preserved through the engineered dissipation, and $|\Psi(0)\rangle$ and $|\Psi(\pi)\rangle$ constitute a pointer basis for a classical bit[13,48–50].

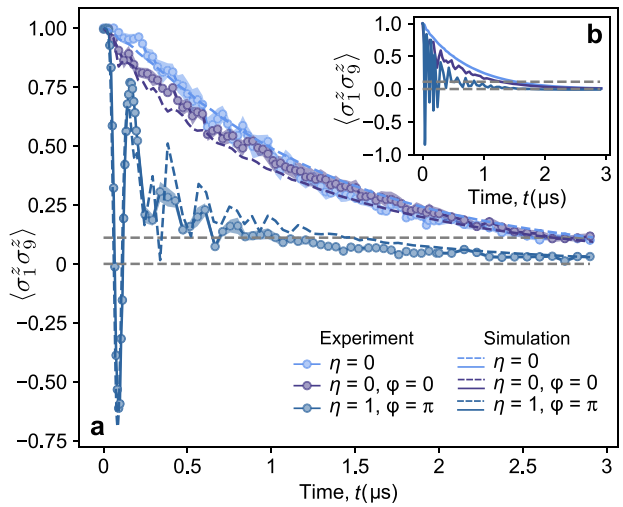

Fig. 4 | The evolution of end-to-end correlation $\langle\sigma_1^z\sigma_L^z\rangle$ on a nine-qubit chain. The shaded regions surrounding the experiment data represent the standard error of the mean over trajectories in the experiment. **a** Three solid lines with circle markers correspond to the initial state $|\phi_0\rangle$, $|\Psi(0)\rangle$, and $|\Psi(\pi)\rangle$, respectively. Dashed lines are numerical simulations with T_1 = 30 μs and T_ϕ = 20 μs. **b** Numerical simulations using the original device parameters without Floquet engineering.

Discussion

We use a discretized SSE to simulate a class of LME by the associated stochastic Hamiltonian, and examine the protocol on a transmon qubit. To observe the multiple steady states in our processor, we harness Floquet engineering to suppress undesired NNN interactions and observe the quantum walk of a Bell state in a superconducting qubit chain. By tuning the phase of the Bell state and activating the dissipation, the end-to-end correlation of a nine-qubit chain converges to the steady value in the symmetry sector $\eta = 0$ or $\eta = 1$. We also show that the phase information in the initial

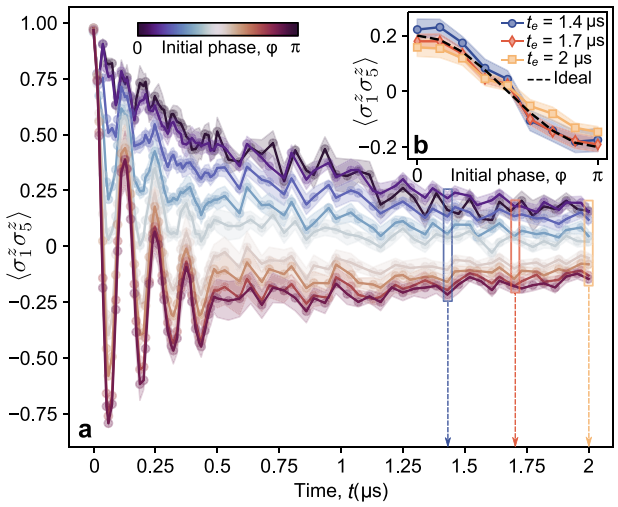

Fig. 5 | The evolution of end-to-end correlation $\langle\sigma_1^z\sigma_L^z\rangle$ for Bell states with different phases on a five-qubit chain. The shaded regions surrounding the experiment data represent the standard error of the mean over trajectories in the experiment. **a** The solid lines with circle markers correspond to the initial phases from 0 to π in increments $\pi/8$, respectively. **b** The values of $\langle\sigma_1^z\sigma_5^z\rangle$ evaluated at t_e = 1.4, 1.7, and 2 μs.

state can be extracted from the steady state in a five-qubit array. While our experiment involves at most nine qubits, numerical analysis of errors and the number of sampling trajectories suggests that our approach can be extended to include more qubits in the same setting (see Supplementary Note 12). Furthermore, our approach can also explore symmetry sectors with $\eta > 1$ by generating multiple pairs of Bell states using digital circuits and further increasing the ratio $U/J_{i,i+1}$ (see Supplementary Note 10)[42]. In addition, our approach could have potential applications in probing the spreading of correlation in open quantum systems[51] and diagnosing non-Markovian dynamics[52].

Methods

Realization of controllable dissipation

We first derive the equation governing the dynamics of the average density operator ρ for a quantum system exposed to the noise. The evolution of the state $|\psi\rangle$ in each trajectory can be described by the following quantum Langevin equation

$$i\frac{d}{dt}|\psi\rangle = H_s(t)|\psi\rangle = \left[H_0 + \sum_{j=1}^{K}\xi_j(t)V_j\right]|\psi\rangle, \tag{8}$$

where H_0 is the dissipationless Hamiltonian, $\xi_j(t)$ is a stationary stochastic process with correlation time τ_c and V_j is a Hermitian operator for $j = 1, 2, \ldots, K$. In the limit $\tau_c \to 0$, Eq. (8) becomes a Stratonovich stochastic equation

$$d|\psi\rangle = -iH_0dt|\psi\rangle - i\sum_{j=1}^{K}V_j|\psi\rangle \circ dW_j(t), \tag{9}$$

where $\circ$ denotes the Stratonovich integral[53] and $\{W_j(t)\}$ are K independent real Weiner processes. Equation (9) can also be converted into an equivalent Itô equation

$$d|\psi\rangle = -iH_{\text{eff}}dt|\psi\rangle - i\sum_{j=1}^{K}V_j|\psi\rangle dW_j(t), \tag{10}$$

where $H_{\text{eff}} \equiv H_0 - \frac{i}{2}\sum_{j=1}^{K}V_j^2$. Following the rules of the Itô integral[54], we have

$$\begin{aligned} d(|\psi\rangle\langle\psi|) = &\sum_{j=1}^{K}V_j|\psi\rangle\langle\psi|V_jdt + (-iH_{\text{eff}}|\psi\rangle\langle\psi|dt \\ &- i\sum_{j=1}^{K}V_j|\psi\rangle\langle\psi|dW_j(t) + \text{h.c.}), \end{aligned} \tag{11}$$

where h.c. denotes the Hermitian conjugate. Hence, the ensemble-averaged state $\rho = \overline{|\psi\rangle\langle\psi|}$ satisfies the following Lindblad master equation

$$\frac{d\rho}{dt} = -i[H_0,\rho] + \sum_{j=1}^{K}V_j\rho V_j - \frac{1}{2}\left\{V_j^2,\rho\right\}, \tag{12}$$

where we have used the property of Itô integral that $|\psi\rangle\langle\psi|$ and $dW_j(t)$ are uncorrelated.

However, generating Wiener processes is challenging, making it impractical to use Eq. (8) to simulate the dynamics described by Eq. (12) in experiments. To address it, we develop an alternative approach by dividing the entire evolution process into N sections, each with a duration Δt. The state $|\psi_n\rangle$ at time $n\Delta t$ is given by the iterative equation

$$|\psi_n\rangle = \exp\left(-iH_0\Delta t - i\sum_j V_j\eta_j^n\sqrt{\Delta t}\right)|\psi_{n-1}\rangle, \tag{13}$$

where $|\psi_0\rangle$ is the initial state, $\{\eta_j^n\}$ are NK independent real random variable satisfying $\overline{\eta_j^n} = 0$ and $\overline{\eta_j^n\eta_l^m} = \delta_{jl}\delta_{mn}$. Expanding Eq. (13) using Taylor's formula and neglecting the high-order infinitesimal terms yields

$$d|\psi_n\rangle \approx \left(-iH_0\Delta t - i\sum_j V_j\eta_j^n\sqrt{\Delta t} - \frac{1}{2}\sum_{j,l}V_jV_l\eta_j^n\eta_l^n\Delta t\right)|\psi_{n-1}\rangle. \tag{14}$$

The corresponding density operator satisfies

$$\begin{aligned} d\rho_n = &-i[H_0,\rho_{n-1}]\Delta t - i\textstyle\sum_j[V_j,\rho_{n-1}]\eta_j^n\sqrt{\Delta t} \\ &+\textstyle\sum_{j,l}\left(V_j\rho_{n-1}V_l - \frac{1}{2}\{V_jV_l,\rho_{n-1}\}\right)\eta_j^n\eta_l^n\Delta t. \end{aligned} \tag{15}$$

Since $\{\eta_j^n\}$ are uncorrelated with ρ_{n-1}, we obtain the master equation for the statistically averaged state $\bar{\rho}$

$$\frac{d\bar{\rho}}{dt} = -i[H_0,\bar{\rho}] + \sum_j V_j\bar{\rho}V_j - \frac{1}{2}\left\{V_j^2,\bar{\rho}\right\}. \tag{16}$$

Therefore, we derive the same master equation from Eq. (13), which is generated by the Hamiltonian

$$H^n = H_0 + \sum_{j=1}^{K}V_j\eta_j^n/\sqrt{\Delta t} \tag{17}$$

within the nth time interval.

In our experiment, the dissipation channels consist of particle pump and loss. When the rates of pump and loss are equal, the dissipation part in the master equation could be rewritten using Hermitian Pauli operators by replacing $\sigma^{\pm}$ with $(\sigma^x \pm i\sigma^y)/2$, yielding

$$\begin{aligned} &\gamma\left(\sigma^-\rho\sigma^+ - \tfrac{1}{2}\{\sigma^+\sigma^-,\rho\}\right) \\ &+\gamma\left(\sigma^+\rho\sigma^- - \tfrac{1}{2}\{\sigma^-\sigma^+,\rho\}\right) \\ &= \tfrac{\gamma}{2}(\sigma^x\rho\sigma^x - \rho) + \tfrac{\gamma}{2}(\sigma^y\rho\sigma^y - \rho). \end{aligned} \tag{18}$$

Hence, combining Eq. (17) and Eq. (18) recovers Eq. (3).

Suppression of NNN interactions by Floquet engineering

By parking the qubits at the frequencies shown in Fig. 3(a), the NNN interactions between pairs Q_1 and Q_3, Q_3 and Q_5, Q_5 and Q_7, and Q_7 and Q_9 are effectively suppressed since the NNN coupling strength ($J_{i,i+2}/2\pi \simeq 1$ MHz) is significantly smaller than the frequency detuning (210 or 330 MHz) between these pairs. The ac flux modulation frequency is set to either 210 or 330 MHz to make the first sidebands of Q_2, Q_4, Q_6, and Q_8 resonate with Q_3 or Q_7. This configuration maintains NNN interactions between Q_2 (Q_6) and Q_4 (Q_8) as their first sidebands align. However, the coupling strength between Q_2 and Q_4 is reduced by a factor of $J_1(\varepsilon_2/\nu_2)J_1(\varepsilon_4/\nu_4) \sim 0.1$ where $J_1(x)$ is the first-order Bessel function of the first kind. A similar reduction occurs for the pair Q_6 and Q_8. Simulation results confirm the presence of multiple steady states under these conditions.

We also introduce a general strategy to fully cancel the NNN interactions in a one-dimensional chain. The fundamental idea is depicted in Fig. S10 of Supplementary Note 6. Our approach involves sequentially applying parametric longitudinal fields with two distinct modulation frequencies, ν_1 and ν_2, to the qubits. Assuming $\nu_1 < \nu_2$, we activate the NN interaction between Q_1 and Q_2 by aligning the first negative sideband of Q_1 with the frequency of Q_2, accounting for the modification of DC offset. Subsequently, we enable the NN interaction between Q_2 and Q_3 by employing a parametric field with modulation frequency ν_2 on Q_2. Following this, a parametric field with modulation frequency ν_1 is applied to Q_3, and similar adjustments are made to other qubits from left to right. Consequently, the NNN interaction between Q_1 and Q_3 can be severed if ν_2 is not an integer multiple of ν_1. This occurs because although both qubits have parametric fields applied with the same modulation frequency ν_1, the frequency detuning between them becomes $\nu_2 + \nu_1$, which cannot be compensated by the modulation frequency. Likewise, the NNN interaction between Q_2 and Q_4 can be eliminated, as their modulation frequency is ν_2, while the frequency detuning between the two qubits is $\nu_2 - \nu_1$. This process can commence from any qubit Q_j in the array, extending from Q_j to Q_1 and Q_j to Q_N. Therefore, by selecting a starting qubit and activating the interaction between Q_i and Q_{i+1} through the first positive or negative sideband of Q_i, we can cancel the NNN interactions between all qubits. The modulation frequencies are chosen by sweeping the T_1 of the qubit near the corresponding sideband.

Data availability

The data that support the findings of this study are available from the corresponding author upon reasonable request.

Code availability

The codes for numerical simulation and data analysis are available from the corresponding author upon reasonable request.

Received: 13 June 2024; Accepted: 30 December 2024;
Published online: 07 January 2025

References

1. Prosen, T. & Pižorn, I. Quantum phase transition in a far-from-equilibrium steady state of an XY spin chain. *Phys. Rev. Lett.* **101**, 105701 (2008).
2. Kessler, E. M. et al. Dissipative phase transition in a central spin system. *Phys. Rev. A* **86**, 012116 (2012).
3. Casteels, W., Fazio, R. & Ciuti, C. Critical dynamical properties of a first-order dissipative phase transition. *Phys. Rev. A* **95**, 012128 (2017).
4. Rota, R., Minganti, F., Ciuti, C. & Savona, V. Quantum critical regime in a quadratically driven nonlinear photonic lattice. *Phys. Rev. Lett.* **122**, 110405 (2019).
5. Heugel, T. L., Biondi, M., Zilberberg, O. & Chitra, R. Quantum transducer using a parametric driven-dissipative phase transition. *Phys. Rev. Lett.* **123**, 173601 (2019).
6. Gong, Z., Hamazaki, R. & Ueda, M. Discrete time-crystalline order in cavity and circuit QED systems. *Phys. Rev. Lett.* **120**, 040404 (2018).
7. Gambetta, F. M., Carollo, F., Marcuzzi, M., Garrahan, J. P. & Lesanovsky, I. Discrete time crystals in the absence of manifest symmetries or disorder in open quantum systems. *Phys. Rev. Lett.* **122**, 015701 (2019).
8. Bakker, L. R. et al. Driven-dissipative time crystalline phases in a two-mode bosonic system with Kerr nonlinearity. *Phys. Rev. Lett.* **129**, 250401 (2022).
9. Vu, D. D. & Das Sarma, S. Dissipative prethermal discrete time crystal. *Phys. Rev. Lett.* **130**, 130401 (2023).
10. Lindblad, G. On the generators of quantum dynamical semigroups. *Commun. Math. Phys.* **48**, 119 (1976).
11. Breuer, H. -P. & Petruccione, F. *The Theory of Open Quantum Systems* (Oxford Univ. Press, 2007).
12. Buča, B. & Prosen, T. A note on symmetry reductions of the Lindblad equation: transport in constrained open spin chains. *New J. Phys.* **14**, 073007 (2012).
13. Albert, V. V. & Jiang, L. Symmetries and conserved quantities in Lindblad master equations. *Phys. Rev. A* **89**, 022118 (2014).
14. Albert, V. V., Bradlyn, B., Fraas, M. & Jiang, L. Geometry and response of Lindbladians. *Phys. Rev. X* **6**, 041031 (2016).
15. Žnidarič, M. Coexistence of diffusive and ballistic transport in a simple spin ladder. *Phys. Rev. Lett.* **110**, 070602 (2013).
16. Popkov, V. & Livi, R. Manipulating energy and spin currents in non-equilibrium systems of interacting qubits. *New J. Phys.* **15**, 023030 (2013).
17. Manzano, D. & Hurtado, P. Harnessing symmetry to control quantum transport. *Adv. Phys.* **67**, 1–67 (2018).
18. Zanardi, P. & Rasetti, M. Noiseless quantum codes. *Phys. Rev. Lett.* **79**, 3306 (1997).
19. Lidar, D. A., Chuang, I. L. & Whaley, K. B. Decoherence-free subspaces for quantum computation. *Phys. Rev. Lett.* **81**, 2594 (1998).
20. Mirrahimi, M. et al. Dynamically protected cat-qubits: a new paradigm for universal quantum computation. *New J. Phys.* **16**, 045014 (2014).
21. Leghtas, Z. et al. Confining the state of light to a quantum manifold by engineered two-photon loss. *Science* **347**, 853 (2015).
22. Touzard, S. et al. Coherent oscillations inside a quantum manifold stabilized by dissipation. *Phys. Rev. X* **8**, 021005 (2018).
23. Lieu, S. et al. Symmetry breaking and error correction in open quantum systems. *Phys. Rev. Lett.* **125**, 240405 (2020).
24. Dutta, S. & Cooper, N. R. Long-range coherence and multiple steady states in a lossy qubit array. *Phys. Rev. Lett.* **125**, 240404 (2020).
25. Dutta, S. & Cooper, N. R. Out-of-equilibrium steady states of a locally driven lossy qubit array. *Phys. Rev. Res.* **3**, L012016 (2021).
26. Roushan, P. et al. Spectroscopic signatures of localization with interacting photons in superconducting qubits. *Science* **358**, 1175–1179 (2017).
27. Zhang, P. et al. Many-body Hilbert space scarring on a superconducting processor. *Nat. Phys.* **19**, 120–125 (2022).
28. Mi, X. et al. Time-crystalline eigenstate order on a quantum processor. *Nature* **601**, 531–536 (2021).
29. Mi, X. et al. Information scrambling in quantum circuits. *Science* **374**, 1479–1483 (2021).
30. Liu, T. et al. Observation of entanglement transition of pseudo-random mixed states. *Nat. Commun.* **14**, 1971 (2023).
31. Barreiro, J. T. et al. An open-system quantum simulator with trapped ions. *Nature* **470**, 486 (2011).
32. Han, J. et al. Experimental simulation of open quantum system dynamics via trotterization. *Phys. Rev. Lett.* **127**, 020504 (2021).
33. Mi, X. et al. Stable quantum-correlated many-body states through engineered dissipation. *Science* **383**, 1332–1337 (2024).
34. Murch, K. W. et al. Cavity-assisted quantum bath engineering. *Phys. Rev. Lett.* **109**, 183602 (2012).

35. Shankar, S. et al. Autonomously stabilized entanglement between two superconducting quantum bits. *Nature* **504**, 419–422 (2013).
36. Fitzpatrick, M., Sundaresan, N. M., Li, A. C. Y., Koch, J. & Houck, A. A. Observation of a dissipative phase transition in a one-dimensional circuit QED lattice. *Phys. Rev. X* **7**, 011016 (2017).
37. Fink, J. M., Dombi, A., Vukics, A., Wallraff, A. & Domokos, P. Observation of the photon-blockade breakdown phase transition. *Phys. Rev. X* **7**, 011012 (2017).
38. Ma, R. et al. A dissipatively stabilized Mott insulator of photons. *Nature* **566**, 51 (2019).
39. Brown, T. et al. Trade off-free entanglement stabilization in a superconducting qutrit-qubit system. *Nat. Commun.* **13**, 3994 (2022).
40. Li, X. et al. Perfect quantum state transfer in a superconducting qubit chain with parametrically tunable couplings. *Phys. Rev. Appl.* **10**, 054009 (2018).
41. Cai, W. et al. Observation of topological magnon insulator states in a superconducting circuit. *Phys. Rev. Lett.* **123**, 080501 (2019).
42. Zhao, S. K. et al. Probing operator spreading via Floquet engineering in a superconducting circuit. *Phys. Rev. Lett.* **129**, 160602 (2022).
43. Budini, A. A. Non-Markovian Gaussian dissipative stochastic wave vector. *Phys. Rev. A* **63**, 012106 (2000).
44. Chenu, A., Beau, M., Cao, J. & del Campo, A. Quantum simulation of generic many-body open system dynamics using classical noise. *Phys. Rev. Lett.* **118**, 140403 (2017).
45. Maier, C. et al. Environment-assisted quantum transport in a 10-qubit network. *Phys. Rev. Lett.* **122**, 050501 (2019).
46. Jordan, P. & Wigner, E. Über das paulische äquivalenzverbot. *Z. Physik* **47**, 631 (1928).
47. James, D. F. V., Kwiat, P. G., Munro, W. J. & White, A. G. Measurement of qubits. *Phys. Rev. A* **64**, 052312 (2001).
48. Zurek, W. H. Decoherence, einselection, and the quantum origins of the classical. *Rev. Mod. Phys.* **75**, 715 (2003).
49. Blume-Kohout, R., Ng, H. K., Poulin, D. & Viola, L. Information-preserving structures: a general framework for quantum zero-error information. *Phys. Rev. A* **82**, 062306 (2010).
50. Macieszczak, K., Guţă, M., Lesanovsky, I. & Garrahan, J. P. Towards a theory of metastability in open quantum dynamics. *Phys. Rev. Lett.* **116**, 240404 (2016).
51. Alba, V. & Carollo, F. Spreading of correlations in Markovian open quantum systems. *Phys. Rev. B* **103**, L020302 (2021).
52. Breuer, H.-P., Laine, E.-M., Piilo, J. & Vacchini, B. Colloquium: non-Markovian dynamics in open quantum systems. *Rev. Mod. Phys.* **88**, 021002 (2016).
53. van Kampen, N. G. Itô versus Stratonovich. *J. Stat. Phys.* **24**, 175 (1981).
54. Øksendal, B. *Stochastic Differential Equations* (Springer, 2003).

Acknowledgements

We thank Giovanna Tancredi for the fruitful discussions. Devices were made at the Nanofabrication Facilities at the Institute of Physics, CAS, in Beijing. This work was supported by: the National Natural Science Foundation of China (Grants No. 11875220, 11904393, 11934018, 12005155, 12047502, 12204528, 92065114, 92265207, and T2121001), Key Area Research and Development Program of Guangdong Province, China (Grants No. 2020B0303030001), Beijing Natural Science Foundation (Grant No. Z200009), Innovation Program for Quantum Science and Technology (Grant No. 2021ZD0301800), Strategic Priority Research Program of Chinese Academy of Sciences (Grant No. XDB28000000), and Scientific Instrument Developing Project of Chinese Academy of Sciences (Grant No. YJKYYQ20200041).

Author contributions

K.X., D.Z., and H.F. supervised the research. T.L. designed the experiment. Z.X. and X.S. fabricated the device. L.L., T.L., and X.-Y.G. performed the experiment and numerical simulations. T.L., L.L., H.F., and Y.-X.Z. wrote the manuscript. All authors contributed to the experimental setup, discussions of the results, and development of the manuscript.

Competing interests

The authors declare no competing interests.

Additional information

Supplementary information The online version contains supplementary material available at https://doi.org/10.1038/s41534-025-00958-6.

Correspondence and requests for materials should be addressed to Tong Liu.